

## DEVELOPMENT OF HIGH FREQUENCY PARTICLE IMAGE VELOCIMETRY TO CHARACTERIZE SEPARATION REGIONS DOWNSTREAM OF A HUMP

J. Fisher, J. Saavedra, G. Paniagua, T. Meyer, M. Slipchenko  
Purdue University  
USA

**Keywords:** high frequency PIV, flow separation, wall mounted hump

### ABSTRACT

Particle Image velocimetry can provide complete planar description of the velocity components in the observation plane. In general, standard PIV techniques provide the flow conditions over a short period of time, based on the laser and camera frequencies. In this article we take advantage of custom designed high-speed lasers to be able to resolve transient flow features with PIV techniques. We focus our analysis on the dynamic formation and oscillation of the separation bubble present behind a wall mounted hump. The test article is used as an analog for the rear suction side of a low-pressure turbine vane operating at low Reynolds Number. The operating envelope of compact air breathing engines is constrained by flow separation under adverse pressure gradients [1]. High fidelity CFD was run on the model to evaluate both steady behavior of the separation bubble as well as unsteady growth from stagnant conditions and response to oscillating pressure fields. Particle Image Velocimetry (PIV) conducted at 2 kHz and 10 kHz is used to evaluate the predictions of these CFD studies. Two operating regimes are considered in the PIV study: steady flow and an oscillating pressure field. The oscillating case is used to scale up to the unsteady flow operation of relevant turbine stages. For the oscillating velocity field an upstream valve is controlled at 2 Hz to induce oscillations on the free stream flow. The dynamic response of the separated flow region under such circumstances is monitored with PIV. Experiments are set-up in a highly modular blow-down wind tunnel facility [2] specifically designed to allow full optical access at the Purdue Experimental Turbine Aerothermal Lab (PETAL).

### NOMENCLATURE

PIV: Particle Image Velocimetry  
LPT: Low Pressure Turbine  
DNS: Direct Numerical Simulation  
RANS: Reynold's Averaged Navier-Stokes  
Nd: YAG: Neodymium: Yttrium Aluminum Garnet doped laser rod  
DMD: Directly Modulate Diode  
AOM: Acousto-Optic Modulator

PETAL: Purdue Experimental Turbine Aerothermal Laboratory

RANS: Unsteady Reynolds Average Navier Stokes

### INTRODUCTION

In decelerating flow regimes, i.e. an adverse pressure gradient, present in most of compressor passages, and in the rear part of the suction side of a turbine airfoil, the near wall flow will tend to detach from the surface geometry and generate a recirculated flow region. In the vicinity of this adverse pressure gradient, the near wall flow slows until it begins to travel backwards with respect to the mean flow. A separation point exists here which splits the flow into two regions; a free stream and a recirculation region. The recirculation region exhibits much higher vorticity than the free stream, as well as showing a near-wall reversal in flow direction. Vortex shedding effects lead to unsteadiness in this region even in inherently steady flow-fields. Between the recirculation and the free stream there is a shear layer which exhibits a high rate of change in velocity. This paper demonstrates the ability to use high frequency PIV to track the height of this shear layer in both steady and transient flows as well as the start-up phase of a sudden flow release wind tunnel. Recently, Hain et al [3] presented results on separation in adverse pressure gradients. Their experiment provided large spatial resolution due to the use of 16 cameras however utilizing a 10 Hz laser limited the results to only instantaneous data with no time resolution. For application to turbomachinery measurements it becomes necessary to use faster acquisition so that transient flow behavior can be tracked, and multiple conditions can be evaluated quickly.

Low Pressure Turbine (LPT) stages have been known to exhibit effects of flow separation for two reasons. The combination of the high altitude, low density flow and the desire to highly load the turbine stage makes the blade airfoil prone to adverse pressure gradient, which cause the flow to separate. When the flow separates in an LPT, a loss of performance is experienced [4]. In order to predict these effects for LPTs, computational methods must be improved. Direct Numerical Simulation (DNS) can predict flow separation well,

but they are still very expensive in terms of computational requirements and not practical to run for multiple geometries in an iterative turbine design process. Less expensive solver methods such as Reynolds Averaged Navier-Stokes (RANS) are more desirable however they are not equipped to model flow separation accurately and cannot resolved the smaller dynamic structures. To gain a better understanding of these flow regimes, empirical studies must be performed.

In the PETAL linear wind tunnel facility, a wall mounted hump made to represent the suction side of an LPT blade was tested at Reynold's Number of 1,490,000. PIV data was taken at 2 kHz and 10 kHz acquisition rate for steady flow, and 2 kHz for oscillating pressure fields. The mean flow and shear layer behavior are tracked and analyzed over time for both conditions.

## TEST SETUP AND DATA ACQUISITION

### 1) Wind Tunnel Facility

The Purdue Experimental Turbine Aero-thermal Laboratory blow down linear wind tunnel was used for the experimental investigation [2]. The facility layout is presented in Figure 1a), 56 cubic meters of dry compressed air are stored at 150 bar. Two different lines divert from the air storage, the first one goes directly to the test cell and discharges the flow in a mixer. The second line goes through a heat exchanger driven by a gas natural burner that provides non-vitiated air at higher flow temperatures. The heated supply is then combined with the cold line in the mixer. The mass flow ratio between the cold and hot lines settles the actual flow temperature. The air is then guided to the facility through a calibrated critical venturi that provides high accuracy mass flow measurements.

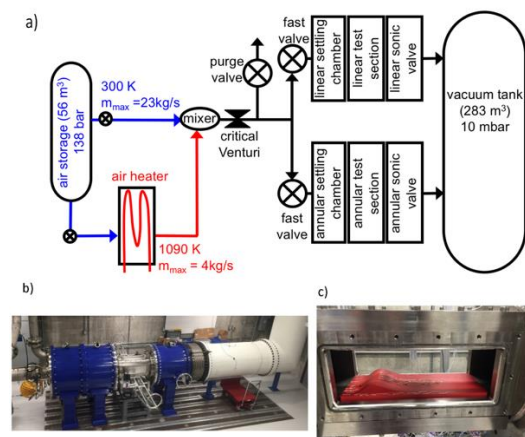


Figure 1: Wind tunnel facility; a) PETAL facility layout, b) Linear wind tunnel, c) Linear test section

During start-up procedures and while achieving uniform flow conditions the air is vented through a purge line. Once the facility operates at steady conditions the purge valve is closed and the valve

upstream of the facility is opened to divert the flow through the linear wind tunnel, as shown in Figure 1b). Finally, the flow is discharged in the vacuum tank through a sonic valve. The use of the sonic valve allows the settlement of the downstream static pressure independently of the vacuum tank conditions. Taking advantage of the sonic valve and varying the mass flow ratio between the cold and hot line the Reynolds and Mach number can be independently adjusted.

### 2) Optical Setup and Laser/Seeding

Two PIV lasers were used to take measurements for this experiment. For long transients such as the flow oscillation and sudden discharge, a continuous, diode-pumped Nd:YAG laser frequency doubled to emit 532 nm light was configured specifically for this experiment from a Raman Laser used in previous biomedical imaging experiments [5]. This continuous laser makes use of a directly modulated diode (DMD) seed laser to produce the laser pulses rather than use two separate laser heads which is common in commercial PIV laser systems. The DMD produces low energy laser pulses at external trigger rate. By constructing the specific pulse train using delay generator, the laser can be configured to produce single, double, or even higher multiple pairs of laser pulses at the 2 kHz operating rate of the system. This configuration is advantageous to the two-headed laser systems commercially used because there is no need to spatially overlap two separate laser sheets which normally can cause uneven and/or misaligned illumination intensities during PIV image acquisition. The 2 kHz laser used is capable of producing 1.25 mJ/pulse when used in this doublet mode. For the measurement region looked at in this experiment, about 7 x 7 cm, the energy is on the lower end of what is required. The laser is being reconfigured to produce more energy for future experiments. Figure 2 shows a schematic of the continuous laser system.

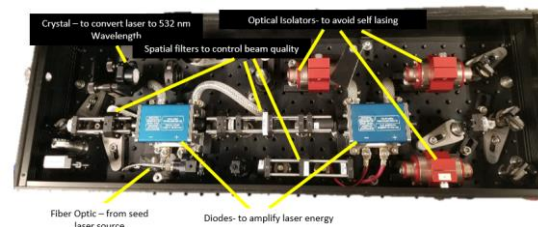


Figure 2: Layout of 2 kHz continuously pulsed laser

For higher repetition rates, a burst-mode Nd:YAG laser was utilized. The pulse selection mechanism for the burst-mode laser is the same as the continuous laser. For amplification of the seed laser, both diodes and flash lamps are utilized. The flash lamps of the burst mode laser allow for much higher amplification of the seed laser to produce higher energy pulses at higher repetition rates. The

limitation of this operation mode is that the lamps can be driven at high energy only for short time to avoid catastrophic failure. The overall burst repetition rate is limited by thermal lensing in the rods due to thermal gradient. This allows the system to fire doublet pulses at 10 kHz, but only for 10 ms long bursts with a 10 second cool down period in between. The maximum pulse energy at 10 kHz is 150 mJ/pulse at 532 nm, which is much higher than needed for PIV measurements. The laser therefore has sufficient pump energy to operate up to 1 MHz rep rate. For the data acquired in this experiment the laser was producing doublets at 10 kHz with 25 millijoules per pulse. Figure 3 shows the layout of the burst mode laser, and its operation is detailed in [6].

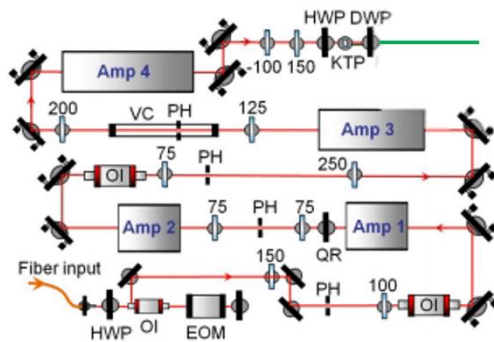


Figure 3: Schematic of burst-mode laser for short duration high pulse energies. Symbols: OI-optical isolator, EOM electro-optic modulator, PH-pinhole, HWP-half-wave plate, DWP-dual-wavelength wave plate, QR-quartz rotator, VC vacuum cell, KTP-Potassium Titanyl Phosphate crystal for 1064nm-532nm conversion. Numbers are focal lengths of spherical lenses.

Both lasers were located in a humidity, temperature and vibration-controlled laser laboratory which is isolated from the test cell where the wind tunnel is located. This prevents the harsh conditions of the wind tunnel from becoming detrimental to the beam quality and energy produced by the lasers. The beam was aligned from the laser lab to a landing optic on an optical table next to the tunnel. From there it was reflected to travel above the wind tunnel on optical rails to be delivered into the test section from the top. The rails provided easily adjustable mounting for mirrors and focusing optics for the laser beam. To produce the PIV sheet, a +1000 mm focal length spherical plano-convex lens was used to focus the beam to its smallest diameter at a height of 8 cm above the surface of the test article. The long focal length spherical lens was chosen to give the sheet a long range of focus to adequately cover the large region of interest observed in this experiment. A -50 mm focal length plano-concave cylindrical lens was used to expand the beam into a sheet. This optic was iteratively adjusted in position along the optical rail to produce the best possible sheet in

terms of width for measurement region size and beam intensity for measurement region illumination consistency. Directly above the test article, a 2" 532 nm coated mirror was placed to reflect the laser sheet downward into the wind tunnel.

The camera for image acquisition was mounted on the same optical rail setup as used for the sheet forming optics. The camera utilized was a Photron Fastcam SA-Z CMOS camera. This system is capable of capturing 1024x1024 images at up to 20,000 FPS, which enables 10 kHz image pairs to be collected with close to microsecond temporal separation between each image pair with 1-megapixel resolution. In this manner, the particle movement could be tracked in short microsecond time scales, while the macro-scale flow motion could be tracked with multi-kHz measurement bandwidth. A Nikon 50 mm lens with an 8 mm extension ring and an aperture of  $f/8$  was used during data collection for excellent depth of focus. The optical rails are fully adjustable in the vertical and axial directions of the wind tunnel, which allows for translation of optics and cameras to select the measurement location of interest. Figure 4 shows a schematic of the optical setup used for data collection.

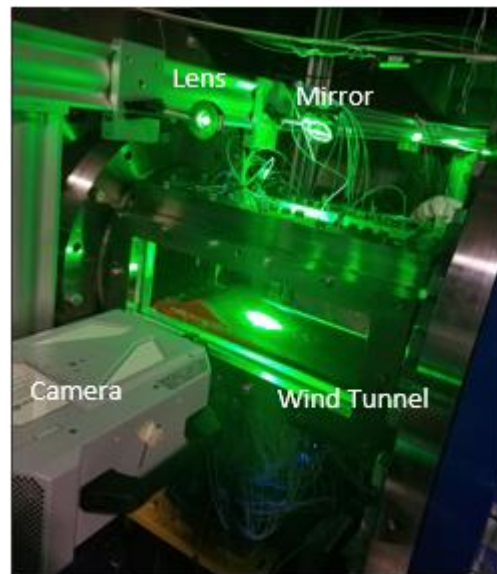


Figure 4: Laser delivery and image acquisition set-up.

For seeding particles, a Concept Smoke Vicount seeding system was used. The system is capable of atomizing 1 ml per second of mineral oil into 1 micron mean diameter droplets. With this output of particle density and size the system is capable of seeding tracer particles in to flows up to 25 kg/s mass flow.

## DATA PROCESSING OF NUMERICAL AND EXPERIMENTAL DATA

### 1) CFD- $k-\omega$ SST – transient flow behavior

Unsteady Reynolds Average Navier Stokes (URANS) simulations were used to characterize the expected performance of the test article at various Reynolds conditions. The solver used for the simulations was Ansys Fluent, taking advantage of the  $k-\omega$  SST transitional model for the turbulence closure. The  $\gamma-\theta$  transitional modeling was used to model the transition of the boundary layer to the turbulent status along the wind tunnel wall upstream of the wall mounted hump. 3D simulations were carried out to identify the main flow features over the test article in the wind tunnel. Figure 5 depicts the numerical domain. The inlet was modelled as a total pressure boundary at 102.1 kPa and total temperature of 296 K. Regarding the turbulence, a turbulence intensity of 5% and a viscosity ratio of 10 were used. The lateral walls: top, bottom, left and right are modelled as isothermal viscous walls at room temperature. Finally, in the outlet a pressure outlet boundary condition is employed to define the static pressure, mimicking the discharge to atmospheric conditions. The pressures and temperatures imposed in the numerical evolution replicate the experimental conditions for the Reynolds/m of  $2.6e^6$ .

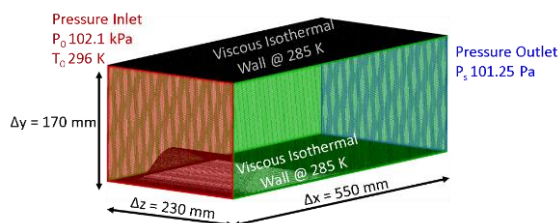


Figure 5: 3D URANS Numerical Domain.

Figure 6a shows the axial velocity contour on the center line of the domain, displaying the separation slightly downstream of the hump summit for the operation at this Reynolds number. The boundary layer detachment has a 2D geometry due to the isolation from the lateral walls achieved by the grooves on the sides of the test article. However, the reattachment is driven by 3D flow structures developed on the downstream side of the hump. Based on the wall pressure measurements displayed in Figure 6b the reattachment takes place at  $x = 0.26$  m. The numerical simulations accurately predict the pressure distribution on the attached flow portion and the separation inception.

### 1) PIV processing

Images were processed using the Lavision Davis commercial software to compute velocity vectors from image pairs. Using a sequential cross-correlation method between two frames, the

program finds the most likely displacement for sets of particles in  $16 \times 16$  pixel regions and the time separation between image pairs to compute the local velocity. A time spacing of 20 microseconds between image pairs was used in the experiment based on an estimate of the optimal particle displacement between measurements based on the expected velocity and pixel size. A calibration image was recorded to convert the measured pixel displacement to distance in meters. A background image of the edge of the geometry was used to register the location of the velocity measurements to the coordinates of the test article. Figure 7 shows an example of the raw data that was processed.

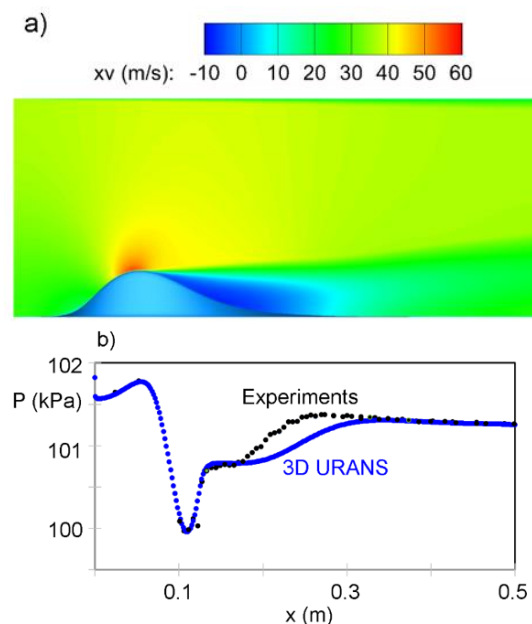


Figure 6: a) Axial velocity in the center plane of the numerical domain from URANS predictions, b) Static pressure distribution in the test article center from URANS and experimental measurements.

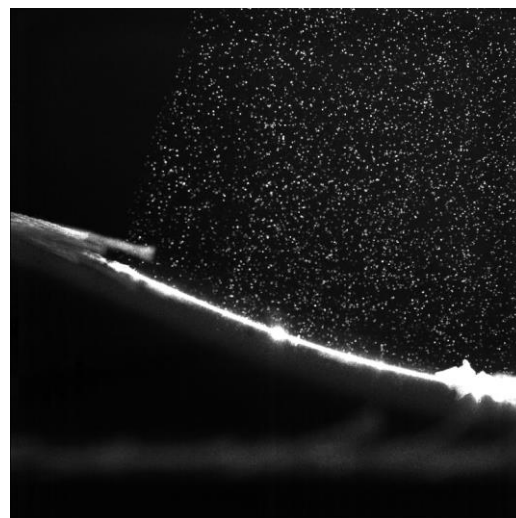


Figure 7: Sample of a raw particle image.

## 2) Flow Structure Resolution

To quantify the behavior of the separated flow region, the images were post-processed in MATLAB. First, the data are rescaled to reflect velocity rather than pixel shift based on calibration images taken prior to the experiment. Then an offset is applied to the coordinate system from the acquisition location so that velocity measurements can be referenced to the test article coordinate system. From the  $V_x$  and  $V_y$  velocity measurements, the velocity magnitude and vorticity are also computed.

With the time history of velocity in the region of interest, the data can be processed to find relevant structures which describe the behavior of the flow. The main feature that is tracked is the shear layer location. Since the shear layer marks the boundary between the free stream flow and the recirculation region, it is used as an indicator to how large of a separation bubble is present in the region of interest. The shear layer is marked by a region of high change in velocity, so tracking  $dV/dy$  can be used to determine the location of this flow feature.

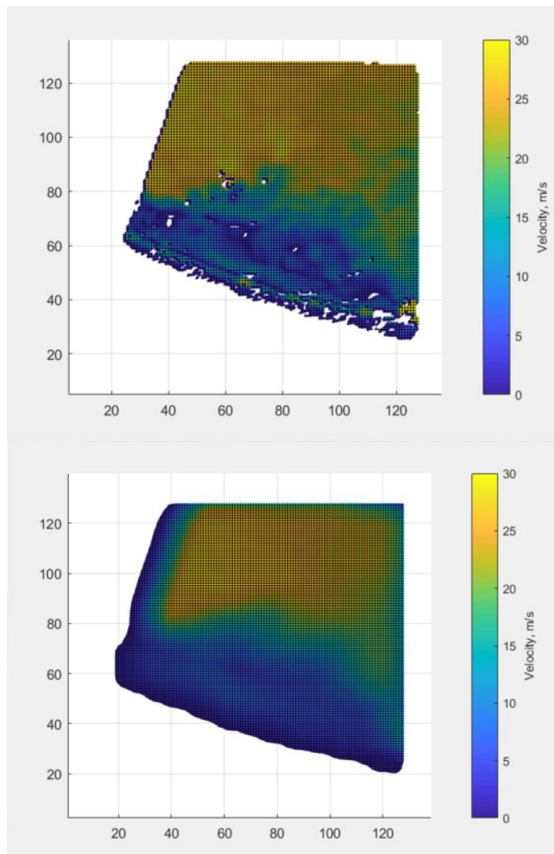


Figure 8: Instantaneous velocity field before, (top) and after (bottom) smoothing.

First, the shear layer function imports a spatial field of velocity measurements. This data is then smoothed to remove non-uniformities that would cause discontinuity in the calculated location of the shear layer. Shown below in Figure 8 is the input

and result of the smoothing filter that is applied to the raw velocity data.

After the data are smoothed, a map of  $dV/dy$  is made for the whole region. This shows better the behavior of the shear layer and recirculation region of the flow field. A clear region exists where the rate of change in velocity is much higher. The code then finds the middle of the shear layer by marking the index where the greatest rate of change occurs. Figure 9 shows the colormap of the velocity gradient. The shear layer can be seen as the yellow spike in the flow field.

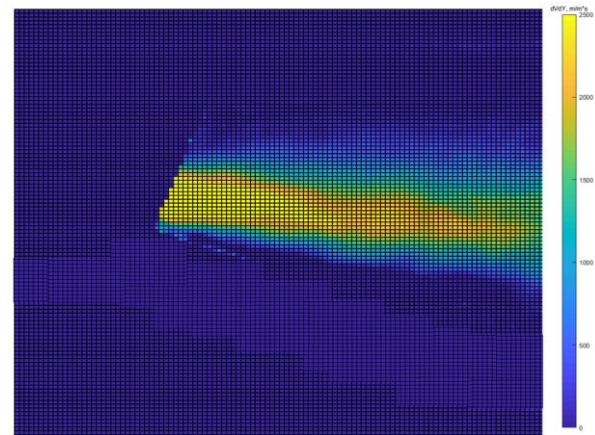


Figure 9: Map of  $dV/dy$  for instantaneous velocity measurement.

## RESULTS AND DISCUSSION

### 1) Steady flow analysis

Shear layer location was tracked for steady flow conditions at both 10 kHz and 2 kHz using the algorithm described above. While the 10 kHz, data was at a higher rate, the length of acquisition was limited to 10 milliseconds total due to the operation of the burst-mode laser. For a flow field with lower frequency dynamics, the burst-mode laser captures only highly dynamic flow features, not being able to resolve lower frequency flow structures.

In order to capture the full cycle of the shear layer evolution in time, the continuous 2 kHz laser was used. Figure 10 displays the evolution of the shear layer (shown as a black line) over time at 10 kHz. Snapshots for four discrete time steps are shown, as well as a time trace of the mean shear layer height for the full 10 millisecond acquisition. As can be seen, there is small fluctuation in the mean height of the shear layer, however there is no large trend that can be observed due to the short nature of the data acquisition.

By utilizing the 2 kHz laser, data can be taken continuously for as long as the camera can capture frames. While the repetition rate is reduced by a factor of 5, many cycles of the flow field behavior can now be captured over 10's of milliseconds or longer. As can be seen in Figure 11, the shear layer

height fluctuates up and down on a time scale that is too long to be captured by a burst-mode laser.

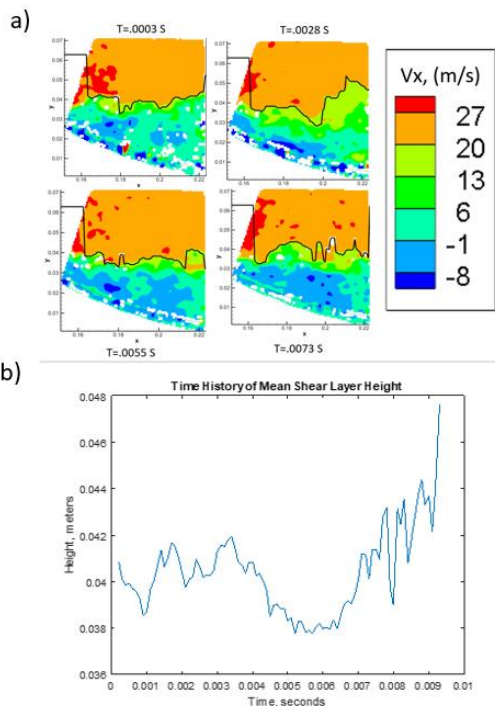


Figure 10: Shear layer height evolution at 10 kHz. a) Four instantaneous images showing shear layer height in black for the whole measurement region. b) Time history of mean shear layer height over the complete acquisition time

With this large time scale acquisition set up, there is no need to take many data points to reconstruct a flow field, and data does not have to be reported in terms of probability density or time averaged senses. A direct time history of values can be analyzed over the evolution of the flow field. This data can then be analyzed for frequency content and coherent structures to give a better sense of the transient behavior of the system.

## 2) Periodic Disturbance

To assess the transient response of the model, the upstream valve supplying air to the test section was controlled to open and close at a repetition rate of 2 Hz. This portion of the experiment served to model the unsteady excitation caused by cyclic blade passing in rotating LPTs. In actual turbines the flow is not steady, and the separation region is constantly perturbed. When the valve is closed, a pressure wave travels from the downstream portion of the test section back to the supply valve. This pressure wave imparts a large deceleration to the flow, causing it to stagnate and then reverse completely. After the valve is re-opened, the pressure wave travels back downstream and through the test section. The flow re-accelerates and then comes to a steady state once again.

Figure 12 shows instantaneous flow fields for streamwise velocity and acceleration values as pressure wave propagates upstream to decelerate the flow.

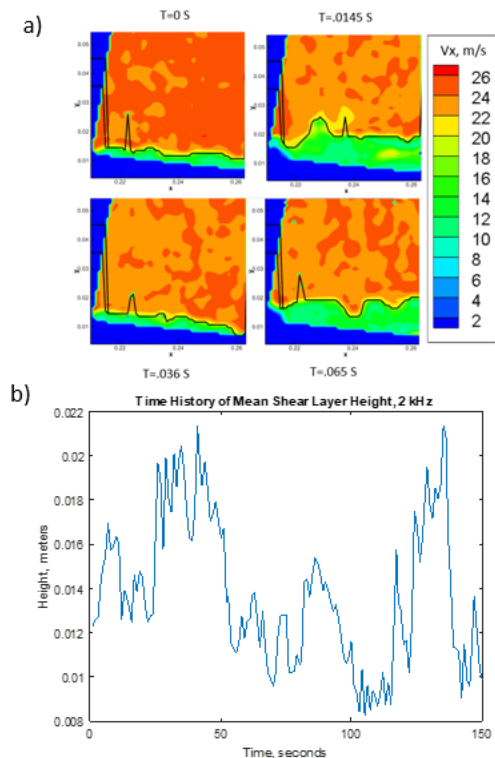


Figure 11: Shear layer height evolution at 2 kHz. a) Four instantaneous snapshots showing shear layer location in black. b) Time history of mean shear layer height for the whole measurement region

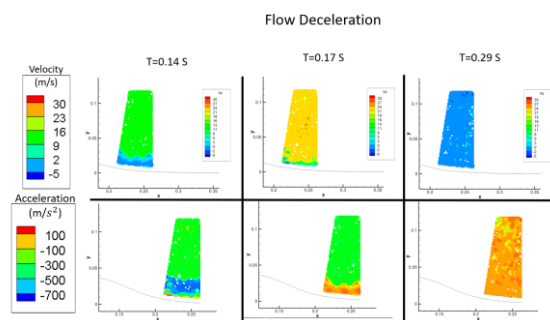


Figure 12: Velocity and acceleration fields during flow deceleration

After the deceleration, there is a small amount of time when the flow travels backward at a relatively small velocity induced by the passing pressure wave. Figure 13 shows the flow behavior after the valve re-opens. There is a strong acceleration which brings the flow back to its steady state condition.

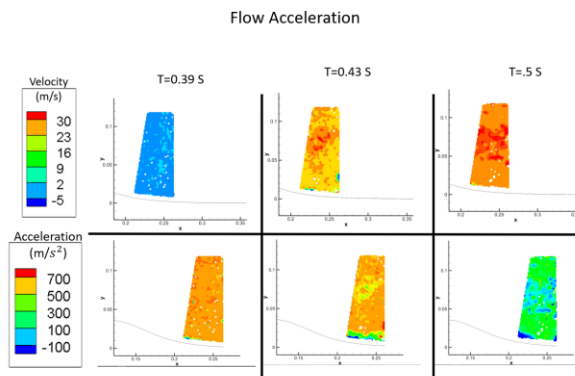


Figure 13: Velocity and acceleration fields during flow acceleration

## CONCLUSION

This paper has presented high resolution, short and long-time scale measurements of separated flow regimes downstream of an ad-hoc designed hump that replicates low-pressure turbines. Processing procedures have been developed to resolve the location of key flow features such as the shear layer which can be correlated to the size of the separated region. Highly transient flows have been measured over multiple cycles in a single acquisition which greatly reduces the number of datasets which need to be recorded. Acceleration of the flow field through large transients have been measured to show the effect of pressure waves traveling through the wind tunnel test section. This work targets the demonstration of rapid testing and verification of many turbine relevant geometries at numerous conditions. The highly modular nature of the wind tunnel coupled with the large amount of optical access presents a fast transition between test articles and configurations to be studied. The short acquisition time required to study complete transient and oscillatory behavior of models means that the facility does not have to be run for long periods of time to build statistics. This means that multiple operating regimes can be studied easily in the same test campaign. The data processing tools enable the quantitative analysis of geometries for performance evaluation to complement and reduce time-consuming simulation.

## REFERENCES

- [1] Saavedra, J.; Paniagua, G.; 2018. "Transient Performance of Separated Flows: Characterization and Active Flow Control". Proceedings of ASME Turbo Expo 2018: Turbomachinery Technical Conference and Exposition, GT2018-75128
- [2] Paniagua G.; Gonzalez Cuadrado, D.; Saavedra, J.; Andreoli, V.; Meyer, T.; Solano, J. P.; Herrero, R.; Meyer, S.; Lawrence, D.; 2018. "Design of the Purdue Experimental Turbine Aerothermal Laboratory for optical and surface aero-thermal measurements". Journal of Engineering for Gas Turbines and Power. DOI: 10.1115/1.4040683. ISSN: 0742-4795.
- [3] Hain, R.; Scharnowski, S.; Reuther, N.; Kähler, Ch.; Schröder, A.; Geisler, R.; Agocs, J.; Röse, A.; Novara, M.; Stanislas, M.; Cuvier, Ch.; Foucaut, J.-M.; Srinath, S.; Laval, J.; Willert, Ch.; Klinner, J.; Soria, J.; Amili, O.; Atkinson, C.; 2016. "Coherent large scale structures in adverse pressure gradient turbulent boundary layers." Conference: 18th International Symposium on the Application of Laser and Imaging Techniques to Fluid Mechanics
- [4] Sanders, D. D.; O'Brien, W. F.; Sondergaard, R.; Polanka, M. D.; Rabe, D. C.; 2010. "Predicting Separation and Transitional Flow in Turbine Blades at Low Reynolds Numbers—Part II: The Application to a Highly Separated Turbine Blade Cascade Geometry". ASME. J. Turbomach. 2010;133(3):031012-031012-7. doi:10.1115/1.4001231.
- [5] Wang, P.; Ma, T.; Slipchenko, M. N.; Liang, S.; Hui, J.; Shung, K. K.; Roy, S.; Sturek, M.; Zhou, Q.; Chen, Z. and Cheng, J. X.; 2014. "High-speed Intravascular Photoacoustic Imaging of Lipid-laden Plaques Enabled by a 2-kHz Barium Nitrite Raman Laser," Scientific Reports, doi:10.1038/srep06889, <https://www.nature.com/articles/srep06889>
- [6] Slipchenko, M. N.; Miller, J. D.; Roy, S.; Gord, J. R.; Danczyk, S. A. and Meyer, T. R.; 2012. "Quasi-Continuous Burst-Mode Laser for High-Speed Planar Imaging", Optics Letters, 37(8), 1346-1348